A BIO-OPTICAL MODEL FOR *SYRINGODIUM FILIFORME* CANOPIES

by

Margaret A. Stoughton
B.S. May 2001, Virginia Polytechnic Institute and State University

A Thesis Submitted to the Faculty of
Old Dominion University in Partial Fulfillment of the
Requirement for the Degree of

MASTER OF SCIENCE

OCEAN AND EARTH SCIENCES

OLD DOMINION UNIVERSITY
May 2009

Approved by:

_____
Richard C. Zimmerman (Director)

_____
Larry P. Atkinson (Member)

_____
David J. Burdige (Member)

ABSTRACT

A BIO-OPTICAL MODEL FOR *SYRINGODIUM FILIFORME* CANOPIES

Margaret A. Stoughton
Old Dominion University, 2008
Director: Dr. Richard C. Zimmerman

Seagrasses are significant ecological and biogeochemical agents in shallow water
ecosystems throughout the world. In many regions, seagrass meadows occupy a
sufficient fraction of the coastal zone, and generate optical signatures that can be
observed from space. Bio-optical models of light absorption and scattering by
submerged plant canopies for certain species such as *Thalassia testudinum* and *Zostera
marina* have successfully modeled the plane irradiance distribution and photosynthesis
within the submerged canopies. *Syringodium filiforme* differs from *T. testudinum* and *Z.
marina*, in leaf morphology and canopy architecture. The objective of this study was to
develop a radiative transfer model that accurately predicts the light absorbed and
reflected by the canopy of this morphologically unique, and abundant tropical seagrass.
The approach involved modifying Zimmerman's (2003) flat leaf bio-optical model by
incorporating the unique vertical biomass distribution of *S. filiforme*. Leaf length
frequency data along with the assumption of a spherical canopy allowed the
parameterization of the unique architecture of the seagrass canopy. Model predictions of
downwelling irradiance and attenuation coefficients within the *Syringodium filiforme*
canopies were consistent with field measurements, therefore providing a robust tool for
predicting photosynthetic performance of these seagrass canopies. Model predictions of
top of the canopy upwelling irradiances, as well as top of the canopy reflectances were

also consistent with field measurements. This predictive understanding will help to develop global algorithms for remote sensing of the abundance and productivity of this species that will lead to better coastal management practices.

ACKNOWLEDGMENTS

TABLE OF CONTENTS

LIST OF TABLES

LIST OF FIGURES

CHAPTER I
INTRODUCTION

The light environment, remotely sensed reflectance, and productivity of natural

ecosystems can be estimated by applying radiative transfer theory (Verhoef & Bach,

2007) which defines the change in energy through absorption, emission and scattering as

photons are propagated through a medium. Within a plant canopy, light can change in

spectral composition as it is transmitted, absorbed and scattered by the canopy structure

(Campbell and Norman, 1998). Modeling radiative transfer processes through vegetation

is highly dependent upon the physical architecture of the plant canopy as well as

individual leaf optical properties which can vary with species and environmental

acclimation. In particular, it is necessary to determine geometric relationships between

the leaf surface and the incoming irradiance distribution because leaves are plane

irradiance collectors that obey the Cosine Law (Campbell & Norman, 1998).

The vertical distribution of leaf biomass required to model radiative transfer

through a plant canopy depends on the structure of the leaves themselves, as well as the

vertical distribution of photosynthetic biomass, which can vary dramatically among

vegetation types (Campbell, 2006). Shrubs may have a photosynthetic biomass

distribution that is, for the most part uniform from the top of the canopy to the ground.

Trees, on the other hand, may have a photosynthetic biomass distribution that is greatest

in the upper layer of the canopy and goes to zero at some distance above the ground.

The model journal for this thesis is Limnology and Oceanography

The photosynthetic biomass of most grasses, including *Phragmites australis,* and seagrasses such as *Thalassia testudinum,* and *Zostera marina* is greatest at the base of the canopy and decreases toward the top, creating a sigmoid shaped distribution curve (Hirose and Werger, 1995; Zimmerman, 2003).

In aquatic habitats, light is attenuated by materials dissolved and suspended in the medium that are independent of the submerged plant canopy (Kirk, 1994; Mobley, 1994). Thus, a predictive understanding of radiative transfer within plant canopies submerged in natural waters requires quantitative knowledge of the inherent optical properties of both the water column and the plant canopy. Understanding radiative transfer in submerged plant canopies provides the basis for calculating rates of photosynthesis and metabolic carbon balance that determines the distribution of plant communities across the submarine landscape and serves as the basis for remote sensing of their optically shallow habitats (Zimmerman, 2006; Dierssen et al., 2003).

Light is one of the most crucial factors controlling the abundance and productivity of seagrasses (Duarte, 1991). All species of seagrass have relatively high light requirements to sustain net productivity when compared to phytoplankton or seaweeds, in large part because they are carbon-limited (Zimmerman et al., 1997; Palacios and Zimmerman, 2007). The high light requirements confine them to shallow waters and makes seagrass vulnerable to eutrophication and sediment loading that decrease light transmission to the benthos (Short and Wyllie-Echeverria, 1996). Light requirements of seagrasses, based mostly on correlative field studies, differ among species and even within species from different locations (Longstaff & Dennison, 1999), but the mechanistic basis for the differences remain elusive. Therefore, a mechanistic

understanding of these differences can be achieved by exploring the fundamental relationships between canopy architecture, individual leaf optical properties and the underwater light environment.

Eutrophication of coastal environments throughout the world, subject seagrasses to intense phytoplankton blooms and suspended sediment concentration that have the potential to cause light limitation that diminishes seagrass habitat. In turn, this can have significant impacts on many species of fish and invertebrates that rely on these "ecosystem engineers" for food and shelter (Short and Wyllie-Echeverria, 1996). In the past three decades, the Florida Bay ecosystem has been dramatically altered, and seagrass communities have been especially hard hit. Large seagrass die-offs have been noticed since 1987, along with an increased turbidity, resulting from ongoing algal blooms and sediment re-suspension (Hall et al, 1999). These die offs of seagrasses or other changes in benthic habitats have been detected from space using satellite imagery and remote sensing, and can be used as indicators of the health of the coastal ecosystem (Dennison et al. 1993). By using remote sensing for rapid identification of benthic features, the prediction of detrimental factors could prove to be useful for coastal management in optically shallow waters (Louchard et al., 2003).

Syringodium filiforme meadows can be found in a variety of environments, such as coastal lagoons, high energy oceanic environments, or somewhat stable hydronamic conditions throughout the southeastern United States, the Caribbean Sea, and the Gulf of Mexico (Kenworthy and Schwarzschild, 1998). Along with *Thalassia testudinum* and *Halodule wrightii*, *S. filiforme* is a major species in Florida Bay, and exists in extreme monospecific (or nearly so) meadows along the Florida Keys. *S. filiforme* is unique

because it posses cylindrical leaves, whereas most seagrasses (i.e. *T. testudinum* and *H. wrightii)* possess flat, strap-like leaves that present a very different optical target to incident light. In addition to their cylindrical shape, *S. filiforme* leaves branch from meristematic nodes located throughout the canopy, rather than the seafloor. This produces a biomass distribution that is more shrub-like than the grass-like patterns of *Thalassia testudinum* or *Zostera marina.* Modeling *S. filiforme* canopies therefore, requires a different approach to estimate productivity, biomass distribution, and vegetation abundance than used previously for seagrass morphotypes characterized by true basal meristems (Zimmerman, 2003). The purpose of this study was to develop a bio-optical model for *S. filiforme* canopies that provides a predictive understanding of the underwater light distribution in these unique canopies and to increase our understanding of radiative transfer processes in different types of seagrass canopies.

CHAPTER II

METHODS AND MATERIALS

A. The bio-optical model of <u>Syringodium filiforme</u> canopies:

The model was based on a two flow approach and consisted of three modules; (*i*) one that simulated the architecture, including leaf geometry of *S. filiforme*, (*ii*) another that calculated the irradiance distribution that results from light absorption and scattering from the canopy architecture and optical properties of the leaves and water column, and (*iii*) a third that calculated photosynthesis of the submerged plant canopy resulting from light absorption by the leaves (Zimmerman, 2003). The model simulated the light environment of a submerged canopy by dividing the canopy volume, including the leaves and the water column, into a series of horizontal sections of finite thickness (Δz). The optical properties of each section were based on the architecture of the canopy, the orientation and optical properties of the leaves, and the optical properties of the dissolved materials and suspended particles in the water column. Some parameters in the model were wavelength and/or depth dependent as indicated by the parenthetic notation; (λ, z). Symbol definitions and their dimensions are listed in Table 1.

Table 1. List of symbols with definitions and units used in the model.

Symbol	Definition	Dimensions
Basic parameters		
z	Depth within the canopy	m
$\bar{\mu}$	Average cosine of plane irradiance distribution	Dimensionless
θ	Polar angle of plane irradiance	Degrees
Canopy architecture		
$B(z)$	Biomass fraction in each canopy layer (z)	Dimensionless
B	Nadir bending angle of the seagrass canopy	Degrees
$h(z)$	Height above the seafloor	m
L	Canopy leaf area index	$m^2\,m^{-2}$
$l(z)$	Leaf area index at depth z	$m^2\,m^{-2}$
$l_p(z)$	Horizontally projected leaf area at depth z	$m^2\,m^{-2}$
t_L	Leaf thickness	m
y	height of individual layer within canopy	m
D	height of the canopy	m
Irradiance within canopy		
$E_d(\lambda,z)$	Downwelling plane irradiance	$W\,m^{-2}nm^{-1}$
$E_u(\lambda,z)$	Upwelling plane irradiance	$W\,m^{-2}nm^{-1}$
Leaf and Canopy optical properties		
$a_L(\lambda)$	Leaf absorption coefficient	m^{-1} leaf thickness
$A_L(\lambda)$	Leaf absorptance	Dimensionless
$D_L(\lambda)$	Leaf absorbance	Dimensionless
$R_L(\lambda)$	Leaf reflectance	Dimensionless
$R_b(\lambda)$	Bottom reflectance of seabed	Dimensionless
$R_u(\lambda)$	Canopy reflectance of upwelling irradiance	Dimensionless
$R_{TOC}(\lambda)$	Top of the canopy reflectance	Dimensionless
Apparent optical properties of the water column		
$K_d(\lambda)$	Water column attenuation of E_d	m^{-1}
$K_u(\lambda)$	Water column attenuation of E_u	m^{-1}
Metabolic parameters		
E_k	Light saturation parameter	mol photon $m^{-2}\,sec^{-1}$
α	Initial slope of P vs. E curve	mol O_2 evolved mol^{-1} photon incident
R	Respiration rate	mol $CO_2\,m^2\,min^{-1}$
$PAR(z)$	Photosynthetically available irradiance in layer z	incident photon m^{-2} leaf
$PUR(z)$	Photosynthetically used irradiance in layer z	quanta absorbed m^{-2} leaf
ϕ_p	Quantum yield of photosynthesis	mol O_2 evolved mol^{-1} quanta absorbed
$P_i(z)$	Biomass-specific photosynthesis in layer z	dimensionless

Module (i): Vertical canopy architecture and leaf geometry

The canopy architecture, leaf orientation and shoot density of six *Syringodium filiforme* populations from Florida Bay were measured in June and July 2006. Shoot density was determined using approximately 20 randomly located quadrats (0.01 m^2) at each station. One shoot consisting of all leaves attached to a single rhizome was collected from each quadrat for subsequent determination of shoot morphology and leaf optical properties. The total surface area per shoot, the number of leaves per shoot, and the maximum length and width of the leaves were measured in the laboratory using a plastic meter tape and digital caliper.

The leaf area index (L) of the entire canopy was divided into a series of fractional leaf area indices $l(z)$ for each depth interval (z) as:

$$l(z) = L \text{ x } B(z) \tag{1}$$

where, L represents the leaf area index for the entire canopy, and $B(z)$ represents the relative biomass at depth z. The relative biomass [$B(z)$] varies at each depth for different species of seagrass and becomes the primary focus for modeling the unique canopy architecture of *S. filiforme*.

The leaf area index (L) for thin flat leaves (such as turtlegrass and eelgrass), is the silhouette, or one-sided area of leaves per unit ground surface area. This leaf area index is also useful for the cylindrical leaves of *S. filiforme* because the shadow area of a cylindrical leaf would be identical to that of a flat, strap like leaf of the same width. Even though the shape and structure of the leaves do not change the calculation of leaf area index, the distribution of leaf origin produces a unique biomass distribution within the *S. filiforme* canopy. The tall and hollow leaves of *S. filiforme* originate at various locations

throughout the canopy, creating a biomass distribution that is considerably different from

other seagrasses in which all leaves emerge from a single meristem in the base of the

shoot at the seafloor.

Leaf orientation relative to the downwelling and upwelling irradiance planes

within the canopy was also accounted for in the model. Unlike phytoplankton, which are

scalar irradiance collectors that harvest light equally from all directions, seagrasses are

plane irradiance collectors in which the geometric orientation of the leaf has a predictable

impact on the light incident on, and therefore, absorbed by the leaf. This relationship is

defined by the Cosine Law, which states that the irradiance incident on a plane surface is

proportional to the cosine of the angle between the photon direction and the surface

normal (Zimmerman & Dekker, 2006). Leaf area index [$l(z)$] within each vertical section

(z), was corrected for orientation by calculating the horizontally projected leaf area [$l_p(z)$]

as a function of the nadir bending angle (β) of the leaves in each depth interval:

$$l_p(z) = l(z) \, \sin\beta(z) \qquad\qquad (2)$$

Also, because seagrass leaves are plane irradiance collectors, the horizontally projected

optical target must be adjusted for the angular distribution of the downwelling or

upwelling irradiance. The cosine law defines this correction as [$l_p(z)$]/$\cos\theta$] for a

collimated beam, where θ represents the zenith angle of the beam incident on $l_p(z)$. Even

though the downwelling light in natural environments is not a collimated beam, its

angular distribution can be approximated using the average cosine ($\bar{\mu}_d$):

$$\bar{\mu}_d = E_d/E_{0d} \qquad\qquad (3)$$

where E_d represents downwelling plane irradiance and E_{0d} represents the downwelling

scalar irradiance. The relationship between seagrass leaves and downwelling irradiance

was approximated by replacing the average cosine for cos θ and using the ratio $[l_p(z)/\bar{\mu}_d(z)]$ as the geometric correction factor (Zimmerman, 2003).

Module (ii): Radiative transfer in a submerged plant canopy

Leaf optical properties (reflectance, transmittance, absorbance, and absorptance) of the cylindrical *S. filiforme* leaves were measured across the visible and NIR spectrum (400-800 nm) using an ASD Field Spec Pro spectrophotometer fitted with an integrating sphere and tungsten lamp. Because *S. filiforme* leaves were narrower than the opening to the integrating sphere, the estimation of leaf optical properties (LOP's) required use of the composite method (Daughtry, 1989), which consisted of carefully arranging four leaves in a custom-made sample holder that separated the leaves by open gaps, across the integrating sphere, and determining the fractional area of the optical window occluded by the leaves. Measured spectral absorbances $[D(\lambda)]$ and reflectances $[R(\lambda)]$ were then corrected by the fractional shadow area to obtain true leaf absorbances $[D_L(\lambda)]$ and reflectances $[R_L(\lambda)]$. Leaf absorbances were measured by placing the leaf sample at the entrance of the integrating sphere between the light source and the sphere. Leaf reflectance was measured by placing the leaves at the back of the integrating sphere so that all of the light scattered backward from the leaf surface was captured inside the sphere. Dependence of $D_L(\lambda)$ on fractional area occupied by the leaves was determined with 2, 3 and with 4 leaves placed in the sample holder, resulting in a linear relationship between absorption and shadow area (cm^2), (slope = 0.039, r^2 = 0.98, n = 4).

Spectrophotometric leaf absorbances $[D(\lambda)]$ were then converted into raw absorptance $[A_{\text{raw}}(\lambda)]$:

$$A_{\text{raw}}(\lambda) = 1 - 10^{-D(\lambda)} \tag{4}$$

and corrected for reflectance $[R_L(\lambda)]$ to get true leaf absorptances $[A_L(\lambda)]$:

$$A_L(\lambda) = A_{\text{raw}}(\lambda) - R_L(\lambda) \tag{5}$$

Corrected leaf absorptances, were converted into length-specific absorption spectra using the cross-sectional thickness of the leaf (t_L) measured using a digital caliper:

$$a_L(\lambda) = -\ln [1 - A_L(\lambda)] / t_L \tag{6}$$

The downwelling and upwelling plane irradiance emerging from each horizontal cross-section of the canopy were then determined by incorporating the leaf optical properties into a two flow model of plane irradiance distribution within the canopy. Downwelling irradiance was calculated using the Lambert-Beer Law:

$$E_d (\lambda, z) = E_d (\lambda, z-1)[1-R_d(\lambda, z)]$$
$$\times \exp [-K_{d(\text{canopy})}(\lambda, z) - K_{d(\text{water})}(\lambda, z)\Delta z] \tag{7}$$

where $E_d (\lambda, z-1)$ represents the downwelling plane irradiance incident on layer z from layer $(z-1)$ above, $[1-R_d(\lambda, z)]$ represents the loss term of upward reflection of the downwelling irradiance in each layer (z). $R_d(\lambda, z)$ was determined from the leaf reflectance $[R_L(\lambda)]$ measured spectrophotometrically in the lab, the horizontally projected leaf area in layer (z), and the average cosine of the downwelling irradiance $[l_p(z) / \bar{\mu}_d (z)]$:

$$R_d(\lambda, z) = R_L(\lambda) [l_p(z) / \bar{\mu}_d (z)] \tag{8}$$

Light attenuation by the canopy $[K_{d(\text{canopy})}(\lambda,z)]$ was calculated from the exponential term $[a_L(\lambda) \times t_L \times (l_p(z)) / \bar{\mu}_d)]$ which incorporates the leaf optical properties within the seagrass canopy where $a_L(\lambda)$ is the geometric absorption coefficient (m^{-1}) for

Syringodium filiforme leaves (Equation 6), t_L is the thickness of the leaves (m), and $(l_p(z)/\bar{\mu}_d)$ is the geometric correction factor as described above for $R_d(\lambda, z)$. The very last part of the equation $[K_{d(water)}(\lambda, z)\Delta z]$ describes light attenuation by the water column and represents the downwelling attenuation coefficient in each layer of the horizontally divided water column and the thickness of each layer in the water column (Δz).

Upward propagation of $E_u(\lambda, z)$ was calculated by reflecting the downwelling irradiance off of the bottom and propagating it back up through the canopy layers in a manner symmetrical to the downward propagation of $E_d(\lambda, z)$, (Zimmerman, 2003):

$$E_u(\lambda, z) = \{[E_d(\lambda, z)R_d(\lambda, z+1)] + E_u(\lambda, z+1)\}$$

$$\times [1 - R_u(\lambda, z)]$$

$$\times \exp[-K_{u(canopy)}(\lambda, z) - K_{u(water)}(\lambda, z)\Delta z] \tag{9}$$

where, $[E_d(\lambda, z+1)]$ represents the downwelling irradiance reflected back up through layer z, $1 - R_u(\lambda, z)$ represents the reflected loss of upwelling light, $E_u(\lambda, z+1)$ represents the upwelling irradiance transmitted through each layer z, $K_{u(water)}(\lambda, z)$ represents the upwelling attenuation coefficient for the water column and was derived from $K_{d(water)}(\lambda, z)$ by propagation of light from the seabed upward through the canopy with the assumption that the seabed represented a Lambertian reflecting boundary (i.e. equal radiances at all hemispheric angles):

$$K_{u(water)}(\lambda, z) = K_{d(water)}(\lambda, z) \frac{\bar{\mu}(\lambda, z)}{0.5} \tag{10}$$

Top of the canopy reflectance (R_{TOC}) was calculated by normalizing the predicted upwelling irradiance emanating from the canopy to the downwelling irradiance incident on the top layer of the canopy where z is equal to zero:

$$R_{TOC}(\lambda, z) = E_u(\lambda, z_0) / E_d(\lambda, z_0) \tag{11}$$

Module (iii): Canopy photosynthesis

The photosynthetic absorptance [$A_p(\lambda)$] was calculated by removing the mean absorption between 710 and 750 nm from $\overline{A}_L(\lambda)$ (defined in Equation 5):

$$A_p(\lambda) = A_L(\lambda) - \overline{A}_L (710\text{-}750) \tag{12}$$

The photosynthetically utilized radiation (PUR) was then calculated for each canopy layer (z) using photosynthetic leaf absorptance, horizontally projected leaf area and upwelling and downwelling irradiances:

$$PUR(z) = \sum_{\lambda} A_p(\lambda) l_p(z) \left[\frac{E_d(\lambda, z-1)}{\overline{\mu}_d(z-1)} + \frac{E_u(\lambda, z+1)}{\overline{\mu}_u} \right] \tag{13}$$

Instantaneous biomass-specific gross photosynthesis within layer (z) [($P_i(z)$) (μmol $O_2\,m^{-2}\,min^{-1}$)] was calculated using a cumulative one-hit Poisson function (Falkowski and Raven, 1997) to provide a general context for evaluating the effects of canopy orientation and leaf optical properties on the potential for photosynthetic light use:

$$P_i(z) = B(z) P_m \{1 - \exp[-\phi_p \times PUR(z)]\} \tag{14}$$

where, $B(z)$ represents the biomass fraction found in layer z, and, ϕ_p represents the quantum yield of photosynthesis (mol C fixed mol^{-1} photons absorbed). The quantum yield of photosynthesis (ϕ_p, mols O_2 evolved mol^{-1} photons absorbed) was determined by the measured relative spectral distribution from the light source and from that, converted *PAR* measurements to *PUR*. In normalizing the photosynthesis versus irradiance (*P* vs. *E*) curves to P_m, the light use efficiency (ϕ_p) became an aggregate term with units of (m^2 leaf s)/(quanta absorbed) and $P_i(z)$ became a dimensionless factor that ranged from 0 to $B(z)$.

The normalized rate of biomass-specific instantaneous photosynthesis for the whole canopy (P_c) was then determined by summation of $P_i(z)$ over z:

$$P_c = \Sigma_z \, P_i(z) \qquad (15)$$

PUR-based predictions of seagrass densities

Predictions of a range of sustainable seagrass densities were estimated using the absorbed light (photosynthetically utilized radiation, *PUR*), that depended on P_m, ϕ_p and A_p. Biomass-specific gross photosynthesis was determined from the *P* vs. *E* curves to provide a basis for relating the leaf orientation within the canopy and the optical properties of the leaves to whole-canopy photosynthesis.

Sustainable seagrass densities were defined as the density at which photosynthesis equals respiration and *PAR*-based calculations for the diffuse attenuation [K_{PAR}] were determined as:

$$K_{PAR} = -\ln \frac{\left(\dfrac{\displaystyle\sum_{\lambda=400}^{700} E_d(z)}{\displaystyle\sum_{\lambda=400}^{700} E_d(0)} \right)}{z} \qquad (16)$$

where, $K(\lambda)$ represents the spectral average of the $K_d(\lambda)$, and λ represents the number of wavelengths. The optical depth for *S. filiforme* canopies was then found as:

$$\zeta = K_{PAR} \cdot z \qquad (17)$$

where z equals the depth at the base of the canopy.

Sustainable seagrass densities were defined as the density at which whole plant photosynthesis equals respiration ($P:R = 1$) on a 24 hour basis, as described by Zimmerman et al. (1997).

B. Model parameterization and validation

Data to validate the model were obtained during two summer field seasons in the Florida Keys in 2005 and 2006 (Fig. 1). Stations north of the Keys represented by the green circles indicate the presence of dense meadows of *S. filiforme* in the relatively turbid waters of Greater Florida Bay. The blue squares represent sand, the pink inverted triangles represent meadows of *T. testudinum.* All stations north of the Keys ranged from 1-2 meters in depth. The red diamonds represent oceanic stations south of the Keys where patchy meadows of *T. testudinum* and *H. wrightii* were present in 7-10 meters of water.

Seabed reflectance spectra [$R_b(\lambda)$] were measured in the lab on sediment cores collected from the *S. filiforme* meadows using a plastic coring cylinder driven into the seabed. The core was then extracted from the sediment along with a few centimeters of the overlying water column and taken back to the laboratory for analysis. Cores were extruded using a worm gear plunger to expose the upper surface layer and remove the overlying water column. Measurements of sediment reflectance were measured using a tungsten light source and ASD spectrophotometer calibrated using a Spectralon (99.9% reflectance) plaque. The reflectance spectra were used to define bottom reflectance [$R_b(\lambda)$] in the model runs.
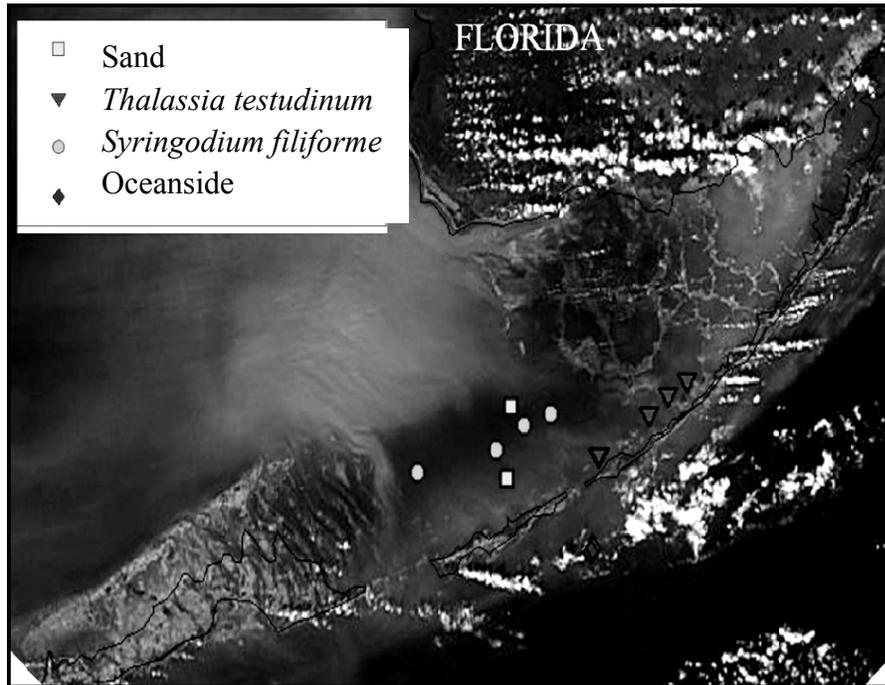
Figure 1. Satellite image of Florida Bay obtained by the MODIS Ocean Color Sensor (http://modis.gsfc.nasa.gov/) showing the field stations occupied in the summer of 2005 and 2006. Circles indicate dense meadows of *Syringodium filiforme*.

Digital light micrographs of individual leaf cross sections of *S. filiforme* and *T. testudinum* were taken with an Axiovert 40 CFL microscope (100x). The cross sections were hand cut using a razor blade, wet-mounted in seawater and illuminated with epifluroescent light (blue excitation) to stimulate chlorophyll *a* fluorescence of chloroplasts with an X-Cite series 120 fluorescence illumination lamp.

In canopy irradiance profiles

Profiles of spectral downwelling and upwelling irradiance through *S. filiforme* canopies were collected using the DOBBS (Diver Operated Benthic Bio-Optical Spectrophotometer), a radiometrically calibrated three-channel HydroRad (HOBI Labs) mounted on a portable frame that was easily manipulated by a SCUBA diver to take *in situ* irradiance measurements with canopies of submerged vegetation. Two of the plane irradiance sensors were mounted on an adjustable wand that could be positioned vertically from 0 to 1.5 meters above the sea floor, providing profiles of downwelling plane irradiance [$E_d(\lambda, z)$] and upwelling plane irradiance [$E_u(\lambda, z)$] within the plant canopy. The third irradiance channel was maintained at a fixed height above the plant canopy to provide reference correction for temporal variation in $E_d(\lambda)$ incident on the canopy during the collection of in-canopy irradiance profiles. The raw in canopy spectra (0.3 nm resolution) were interpolated to 1 nm intervals using a cubic spline and smoothed using a 10 nm boxcar running average for validation against the model and adjusted for any temporal variation in $E_d(\lambda,0)$ above the canopy.

Water column optical properties:

Values of $K_d(\lambda, z)$ and $\bar{\mu}$ for the water column were obtained using an HR4 field Spectroradiometer (HydroRad 4 Spectroradiometer HOBI Labs, Inc.) fitted with two Gershun sensors and two plane irradiance sensors. The HR4 was mounted on a portable frame and placed on the seafloor in a clear area away from the seagrass canopy. Two of the Gershun sensors were located 1 meter above the sea floor and measured downwelling

$[E_{0d}(\lambda)]$ and upwelling $[E_{0u}(\lambda)]$ scalar irradiance. Total scalar irradiance was then calculated:

$$E_0 (\lambda) = E_{0d}(\lambda) + E_{0u}(\lambda) \tag{18}$$

One of the two plane irradiance sensors (E_{d2}) was located beside the Gershan sensors; the other was located 1 meter below E_{d2} (E_{d1}). The coefficient of downwelling light attenuation [$K_d(\lambda)$] was then calculated from Beer's Law as:

$$K_{d(water)}(\lambda) = \frac{-\ln \dfrac{E_{d1}(\lambda)}{E_{d2}(\lambda)}}{z} \tag{19}$$

where the vertical distance between the two sensors (z) was 1 m. The average cosine of the zenith angle of all downwelling light ($\bar{\mu}_d$) (Kirk, 1994) was then calculated as:

$$\bar{\mu}_d = \frac{E_d(\lambda)}{E_{0d}(\lambda)} \tag{20}$$

Irradiance measurements from each of the four sensors were recorded at 0.35 nm increments every 5 minutes. The values of $K_{d(water)}(\lambda)$ taken at each station, along with the $E_d(\lambda, TOC)$ values taken from the DOBBS at each station at the top of the canopy were used to initialize the model runs (Eq. 7).

Photosynthesis and respiration of individual leaf (photosynthetic tissue) and respiration of non-photosynthetic segments rhizome segments were measured using a temperature-controlled polarographic oxygen electrode system filled with 5 ml of 0.2 μm filtered seawater. Leaf segments were first incubated in total darkness to measure respiration, and then exposed to a range of increasing light intensities created using neutral density filters and a tungsten fiber-optic light source and calibrated using a Biospherical *PAR* sensor. Rates of oxygen consumption/evolution at each light level

were calculated as the time-rate-of-change from linear portions of the digitally recorded oxygen concentration time series.

Metabolic data were fit to the cumulative one hit Poisson function:

$$P = P_{\mathrm{m}}(1 - e^{-\alpha E/P\mathrm{m}}) - R \tag{21}$$

where P_{m} represents the maximum, or light saturated rate of gross photosynthesis, E represents the incident irradiance (PAR), α represents the light-limited slope of the P vs. E curve, and R represents dark respiration. The P vs. E curve parameters (P_m, α and R) were estimated using a direct fit algorithm for non-linear models implemented using Sigma Plot 10.0 that provided objective error estimates (Zimmerman et al., 1987) and were compared to model output estimates. The quantum yield of photosynthesis (ϕ_p) was calculated by first converting PAR to $E(\lambda)$ and PUR was then determined from Equation 13. Finally, P vs. PUR was plotted just like the P vs. E curves and (ϕ_p) was determined as the slope of the linear portion of the curve.

The modeled upwelling and downwelling irradiances were compared to field measurements of in-canopy $E_d(\lambda,z)$ and $E_u(\lambda,z)$ obtained by the DOBBS at discrete locations within the canopy using % RMS (root mean square) error:

$$\%RMS = \sqrt{\frac{1}{n}\sum_{\lambda=1}^{n}\frac{(DOBBS(\lambda) - Modeled(\lambda)^2}{DOBBS(\lambda)}}x100 \tag{22}$$

where n equals the number of wavelengths, $DOBBS$ (λ) is the measured $E_d(\lambda)$ taken from the field measurements and $Modeled(\lambda)$ is the predicted $E_d(\lambda)$.

CHAPTER III

RESULTS

Leaf optical properties:

The mean absorption (a_L) and absorptance spectra (A_L) of *S. filiforme* was quantitatively similar to flat-leaf species, such as *T. testudinum* and *Z. marina*, in the blue (400-500 nm) and red (600-700 nm) portions of the visible spectrum (Fig. 2a). However, the *S. filiforme* spectrum was two to three times more absorbent in the green (500-650 nm), and therefore less spectrally sensitive (optically gray) than is typical of most green plant leaves, including other seagrasses like *T. testudinum* and *Z. marina*. Although the leaves of *S. filiforme* absorb about 75% of the incident light, the photosynthetic pigments are responsible for only about 22% of the absorption. In contrast, *T. testudinum* absorbs about 46% of the incoming light, and 31% of the incident light is absorbed by photosynthetic pigments. *Z. marina* absorbs about 63% of the incoming light and 46% is absorbed by the photosynthetic pigments.

Despite the differences in absorption spectra, leaf reflectance spectra (R_L) of *S. filiforme* were virtually indistinguishable from *T. testudinum*, and *Z. marina* (taken from Zimmerman, 2003) across most of the spectrum. There was a clear peak in the green between (500-600 nm) and a distinct "red edge" starting at 700 nm and extending to the near infrared (NIR) (Fig. 2b). *T. testudinum* leaves, however, were slightly more reflective in the green, (525 to 650 nm).
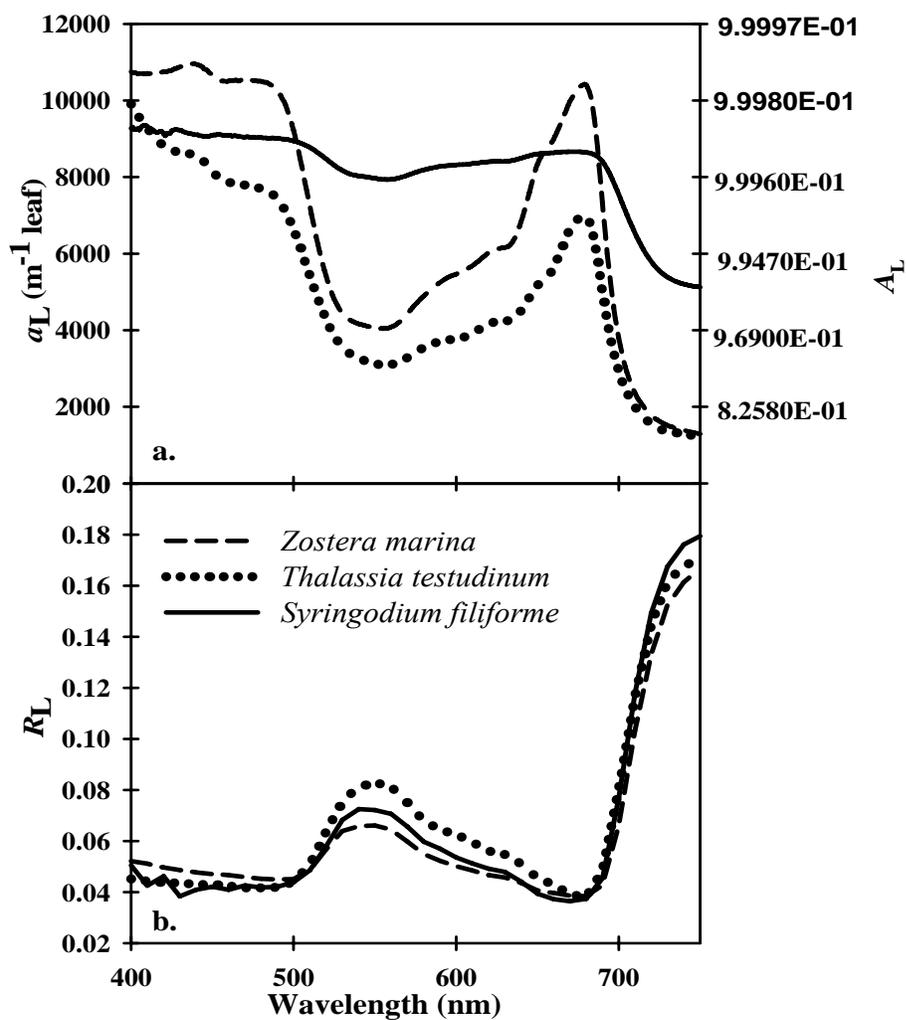
Figure 2. (a) Mean leaf absorption [$a_L(\lambda)$ m^{-1} leaf] and leaf absorptance (A_L) spectra of *Syringodium filiforme*, *Thalassia testudium* and *Zostera marina*. **(b)** Mean leaf reflectance (R_L) spectra of *S. filiforme*, *T. testudium* and *Z. marina*. Data from *T. testudinum* and *Z. marina* are from Zimmerman (2003).

Epiflouresent cross sections of *S. filiforme* and *T. testudinum* revealed the chloroplasts (fluorescent red bodies) within *S. filiforme* to be widely dispersed in the epidermal layer and mesophyll up to three cell layers away from the leaf surface, which comprises about 47% of the total leaf volume whereas, chloroplasts within *T. testudinum* and most other flat-bladed seagrasses are packed into two single-cell layers of the epidermis comprising only about 27% of the total leaf area (Fig. 3). The cross section of *S. filiforme* also reveals that about 44% of the volume was devoted to large air lacunae (buoyant air channels) whereas the lacunae within *T. testudinum* comprise only about 12% of the leaf volume. These large air spaces may increase light refraction within the leaf, increasing the probability of light absorption (Lee, 1986).
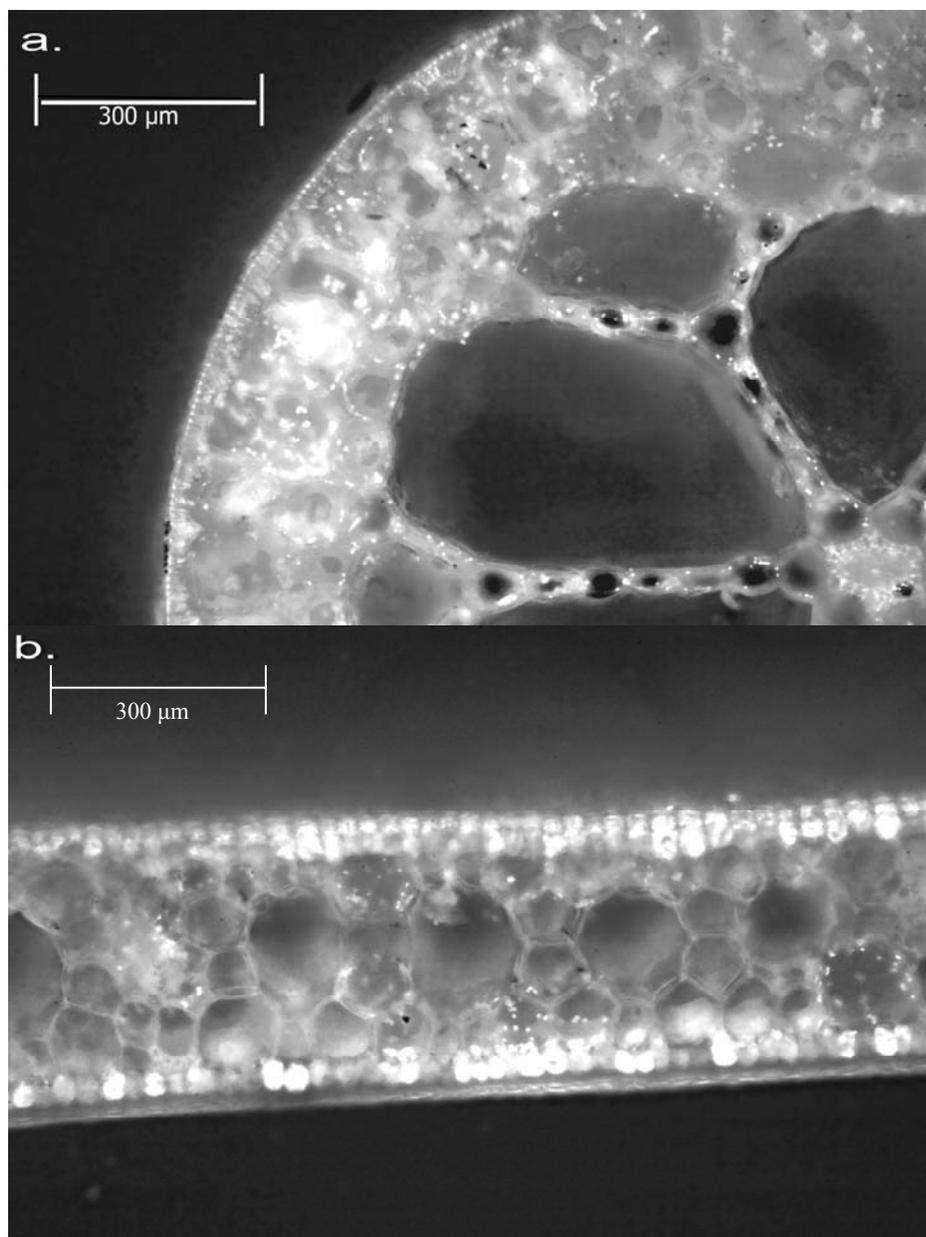
Figure 3. (a) Epifluorescence micrograph showing partial cross section of a *Syringodium filiforme* leaf. Chloroplasts appear as bright objects within the outermost three layers of cells. **(b)** Epifluorescent micrograph showing the cross section of *Thalassia testudinum* leaf. Chloroplasts were almost completely restricted to the outermost epidermal cell layer.

Seabed optical properties:

Reflectance spectra $[R_b(\lambda)]$ of the seabed below the *S. filiforme* canopies had qualitatively similar shapes across all stations, with $[R_b(\lambda)]$ increasing from blue to red (Fig. 4). Peak reflectance at 640 nm ranged from about 0.12 to 0.26 which was about half of the bottom reflectance for the highly reflective ooitic carbonate sand reported by Zimmerman, (2003) (~0.45 at 650 nm). The spectra also exhibited a distinct dip at 670 nm, probably due to absorption by chlorophyll containing microalgae growing on the sediment surface.
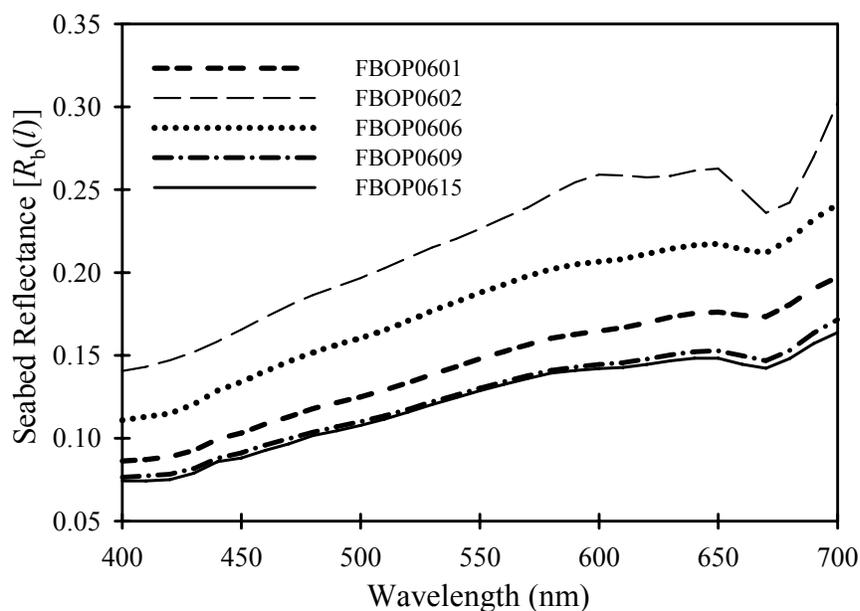
Figure 4. Mean reflectance spectra of sediment cores collected at five Florida Bay stations where dense *Syringodium filiforme* canopies were observed.

Sensitivity of the model to canopy architecture:

The first simulation of canopy structure and biomass distribution for *S. filiforme* canopies followed a sigmoid model, in which most of the biomass was located at the seafloor and decreases exponentially upward to the top of the canopy:

$$B(z) = \frac{\psi}{1 + \left[\dfrac{h(z)}{I}\right]^{s}} \tag{23}$$

B(*z*) represents the relative biomass in layer *z* of the canopy, ψ is the fraction of biomass at the seafloor, [*h*(*z*)] is the height above the seafloor, *I* represents the intermediate point within the canopy where the curve shifts from concave to convex, and *s* represents the exponential shape factor (Zimmerman, 2003). Values of ψ, *I,* and *s* were fitted to vertical biomass distributions derived from leaf size-frequency data for all stations taken in 2005 and 2006 (Fig. 5). From this point on, FBOP0606 will be used as an example station, for simplicity, because results from other stations were similar to this station.
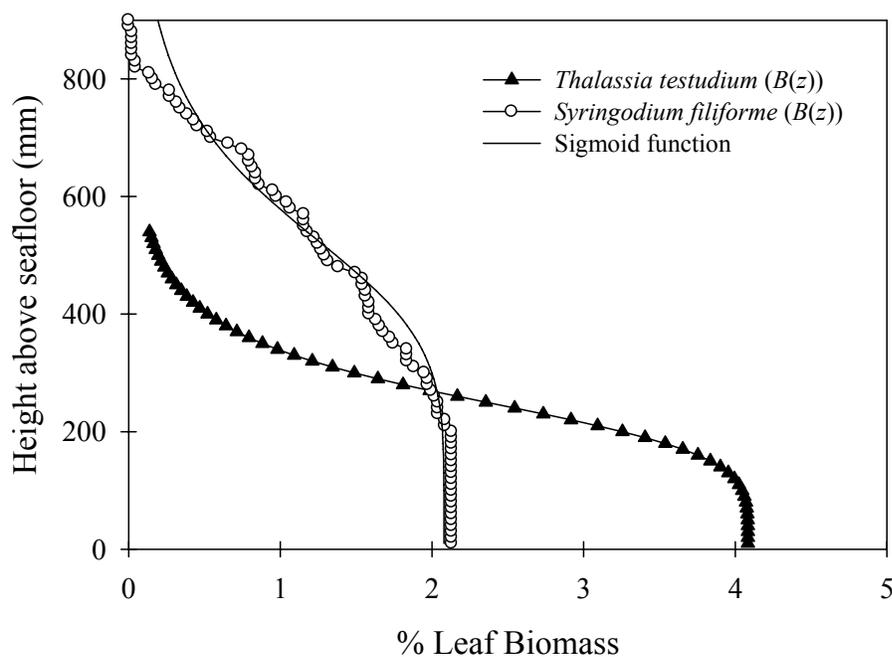
Figure 5. Vertical biomass distribution of *Syringodium filiforme* compared to *T. testudium* taken near Lee Stocking Island, Bahamas (Zimmerman, 2003). The sigmoid distribution curve was fitted to *S. filiforme* to derive the biomass distribution parameters for the sigmoid model.

The sigmoid biomass model generated downwelling irradiance spectra that were within 12% of observed values at the bottom of the canopy (Fig. 6). The model, however, overpredicted upwelling irradiances by 34% at the top of the canopy (550 mm), 27% in the middle (350 mm), and 50% at the bottom of the canopy (200 mm), (Fig. 7).
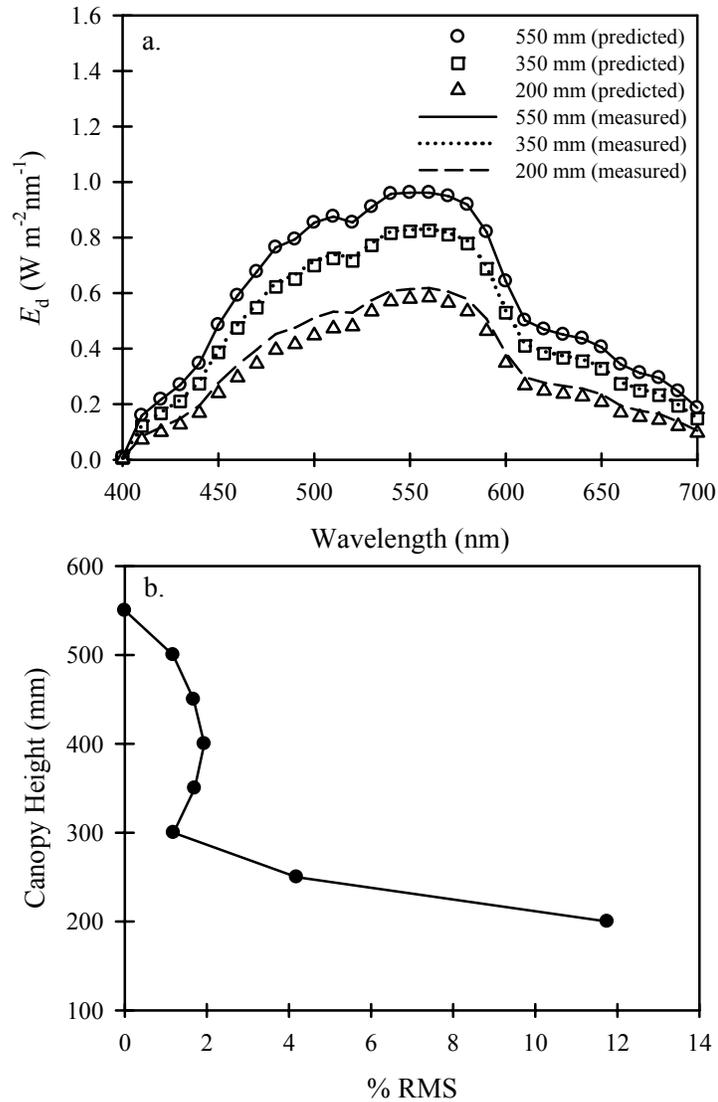
Figure 6. (a) Predicted vs. measured downwelling irradiance $[E_d(\lambda)]$ using original vertical biomass distribution parameters for flat strap-like leaves (sigmoid model) at the top of the canopy (550 mm, initial condition), in the middle of the canopy (350 mm), and towards the bottom of the canopy (200 mm). **(b)** % RMS of predicted vs. measured E_d using the sigmoid biomass distribution parameters for all simulated and measured depths within the canopy.
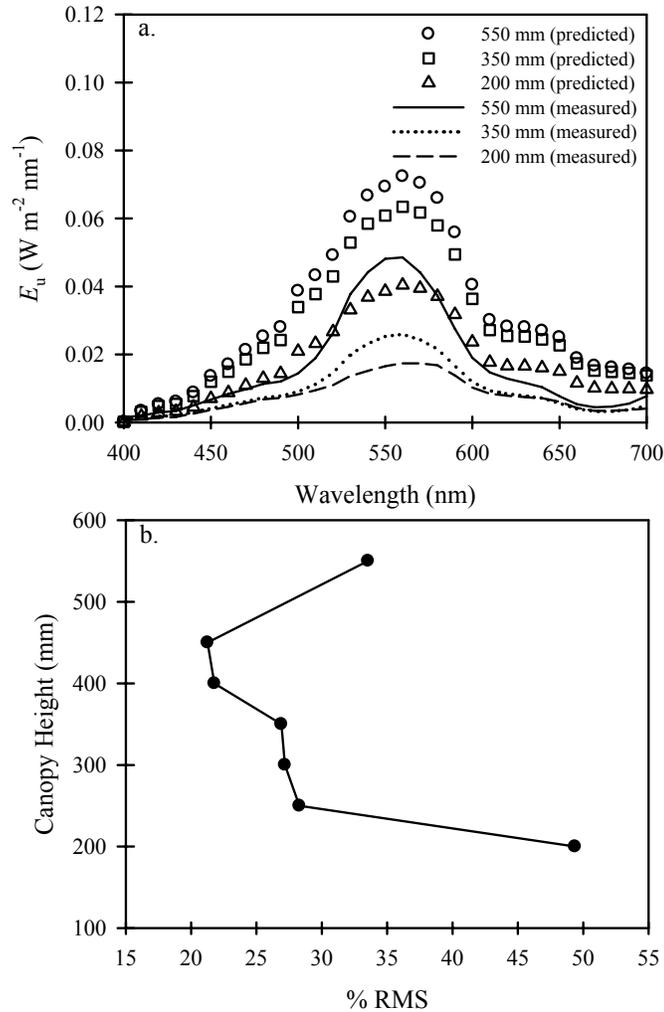
Figure 7. (a) Predicted vs. measured upwelling irradiance (E_u) using original biomass for flat strap-like leaves (Sigmoid model). **(b)** % RMS of predicted vs. measured E_u using the original sigmoid biomass distribution parameters.

Although the average recorded length for *S. filiforme* shoots measured in the laboratory was 754 mm, the realized average height of the submerged canopies was only 550 mm. Consequently, a set of biomass coefficients were created to compress the canopy by bending the leaves at several different heights from 0 to 550 mm above the

bottom causing the leaves in the upper layer to be denser and more horizontal than below

the bending point (Fig. 8). Compression of the canopy at each 100 mm increments

therefore provided biomass distributions that were much different than the fully extended

sigmoid model (Fig. 9).
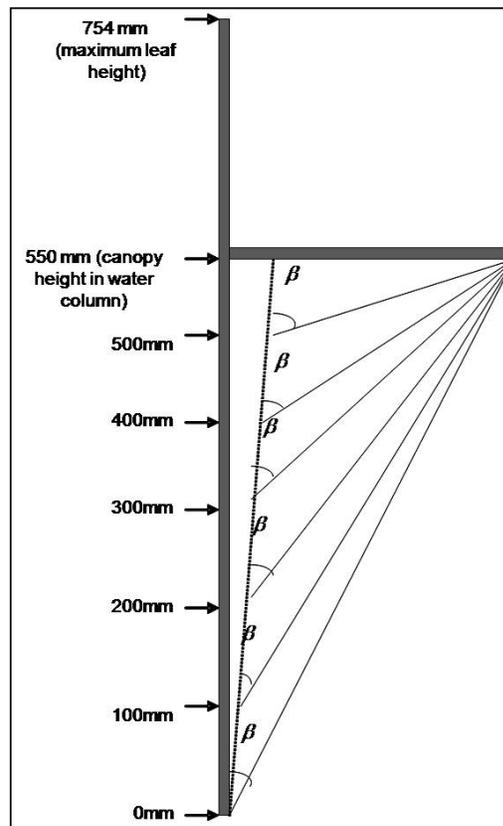
Figure 8. Schematic of compressed sigmoid model. To increase the accuracy of the E_u

predictions from the model, new biomass coefficients were created by compressing the

height of the canopy at 100 mm intervals where β represents the bending angle. Biomass

distribution parameters were derived using the sigmoid model with compression of h(z),

thereby altering the intermediate point (I) as well as the shape factor (s). These

parameters were then applied to the compression model runs.
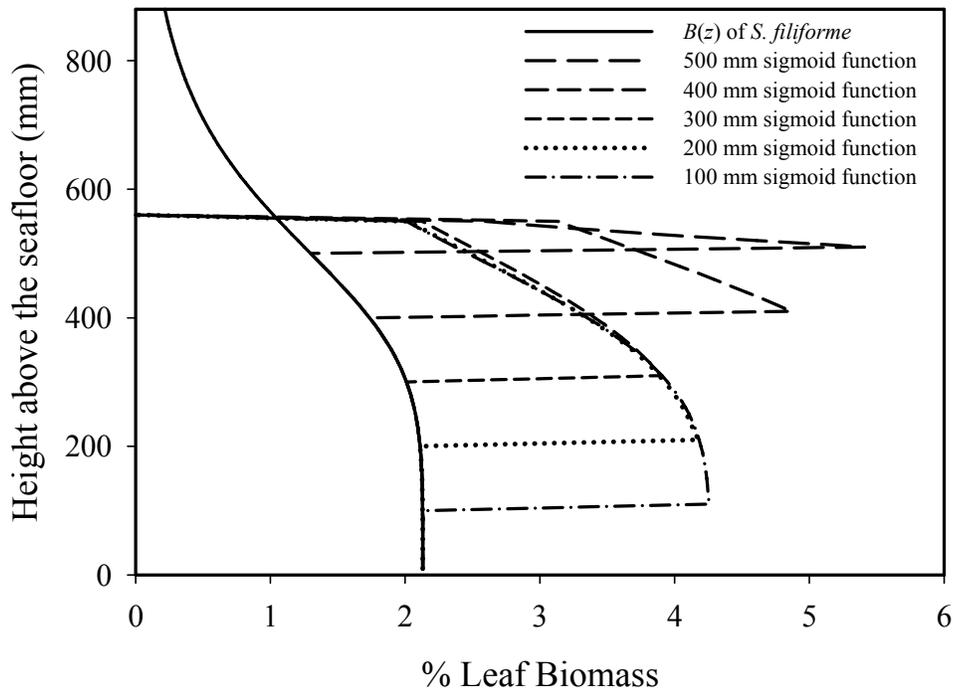
Figure 9. % Leaf Biomass vs Height above the seafloor using the compressed sigmoid model and bending canopy height by 100 mm increments to obtain the vertical biomass parameters.

The biomass distribution parameters were derived using the same sigmoid model as for the fully extended (754 mm) canopy and applied to each of the model runs. However, bending the canopy at 100 mm increased the underprediction of E_d to 78% and 97% RMS in the middle and bottom of the canopy, respectively (Fig. 10a). Bending at 300 mm further increased the underprediction of E_d to 96% and 93% RMS in the middle and bottom of the canopy, respectively (Figure 10a). Bending at 500 mm reduced the

underprediction of E_d to 54% and 32% RMS in the middle and bottom of the canopy,

respectively (Figure 10a). Bending at 500 mm also resulted in a better prediction of E_d at

the middle and bottom of the canopy compared to bending at 100 mm and 300 mm.

Bending the biomass at 100 mm also increased the underprediction of the E_u at the top,

middle and bottom of the canopy (Figure 10b), relative to the fully extended (754 mm)

sigmoid model. Bending at 300 mm also underpredicted E_u by 37%, 79%, and 97% in

the top, middle and bottom of the canopy, respectively (Figure 10b). Bending the canopy

at 500 mm reduced the underprediction of E_u at the top, middle and bottom by 2% (Fig.

10b.) As with the E_d, the bending at 500 mm resulted in a better prediction of E_u in the

middle and bottom of the canopy when compared to bending at 100 mm and 300 mm.

These results indicate that the model is sensitive to changes in biomass

distribution resulting from differences in canopy height and bending position. Further,

bending this canopy at 500 mm rather than 100 mm or 300 mm, resulted in more accurate

predictions of irradiance distribution especially within the middle and bottom portions of

the canopy. Overall, the compressed sigmoid model did not simulate the E_d and E_u as

well as the fully extended sigmoid model despite the fact that it more accurately

represented the true height of the submerged plant canopy.
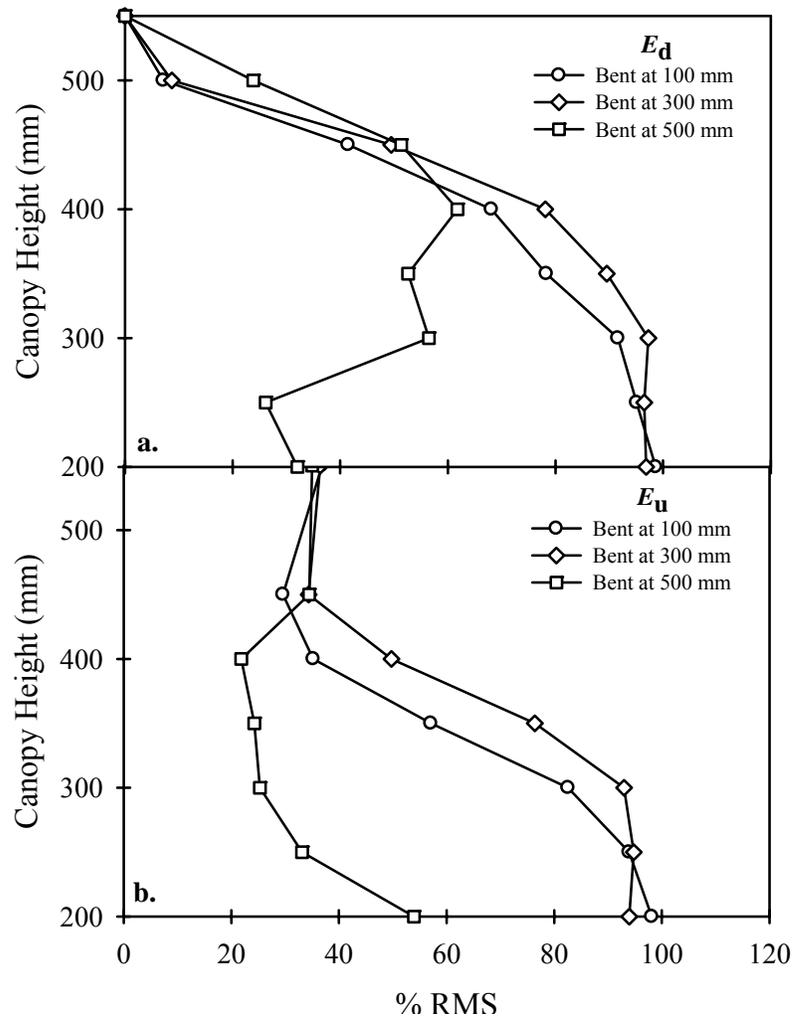
Figure 10. (a) % RMS of predicted vs. measured E_d compressed at 100, 300 and 500 mm increments. **(b)** % RMS of predicted vs. measured E_u compressed at 100, 300 and 500 mm increments.

The undifferentiated branching architecture of *S. filiforme* suggests that its canopy is geometrically different from most of the seagrasses, including *T. testudinum* and *Z. marina,* on which the sigmoid distribution was based. Unlike the sigmoid model, which assumes all leaves originate at the seafloor, the leaves of *S. filiforme* originate at branch

points throughout the canopy, which distributes a larger fraction of biomass in the middle

and upper portions of the canopy (Fig. 11). To simulate this spherical distribution, the

relative biomass distribution [$B(z)$] within each vertical layer of the canopy was

calculated from the partial volume (V_1) of a sphere where, y_1 represents the height (m) of

an individual layer in the spherical canopy, and D represents the height (or diameter) of

the entire spherical canopy:

$$V_1 = \pi/3 \times y_1{}^2 \times (1.5D - y_1), \tag{24}$$

$$V_2 = \pi/3 \times y_2{}^2 \times (1.5D - y_2), \tag{25}$$

$$B(z) = \Delta V_1 - \Delta V_2 \tag{26}$$

The resulting fractional biomass within each vertical layer of the canopy [$B(z)$] was

calculated by subtracting the partial volume of the sphere (ΔV) below the layer from the

volume including the layer (Figure 11):

$$B(z) = 4.57 \times 10^{-7} + 9.10 \times 10^{-5} \times h + {-1.14 \times 10^{-7}} \times h^2 \tag{27}$$

where, h represents the height of the canopy in mm. As with previous simulations using

the sigmoid distribution, canopy height was constrained to 550 mm to correspond to

heights observed in the field.
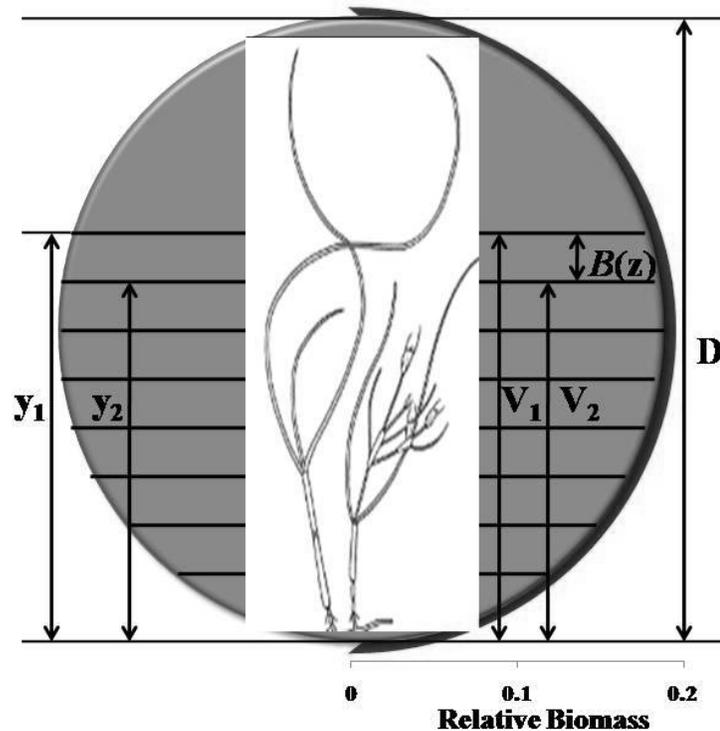
Figure 11. Spherical model representation of canopy architecture and vertical biomass distribution within *S. filiforme* canopies. Relative biomass distribution [$B(z)$] within each vertical layer was calculated by using the partial volume (V_1) of a sphere where, y_1 represents the height (mm) of an individual layer in the canopy (or sphere), and D represents the height of the entire canopy or sphere. The vertical biomass distribution was then fit to a second order polynomial curve (bold line).

Both modeled and measured E_d (λ, z) decreased down through the canopy (Fig. 12a). The model generated % RMS errors of E_d of 23% and 17.5% in the middle (350 mm) and the bottom (200 mm) of the canopy, respectively (Fig 12b). The model also under predicted the E_d in the middle and the RMS error of 23% was considerably higher than the original sigmoid model simulating the 800 mm canopy. However, the RMS error for

E_d was 54% less than the compressed sigmoid model bent at 100 mm, 69% less than the

compressed sigmoid model bent at 300 mm, and was 30% less than the compressed

sigmoid model bent at 500 mm. The spherical model also slightly under predicted the E_d

at the bottom (200 mm) of the canopy but the RMS error of 18%, was only 6% higher

than the original sigmoid model and 78% less than the compressed sigmoid model bent at

100 mm, 75% less than the compressed sigmoid model bent at 300 mm, and was 14%

less than the compressed sigmoid model bent at 500 mm (Fig. 12b).
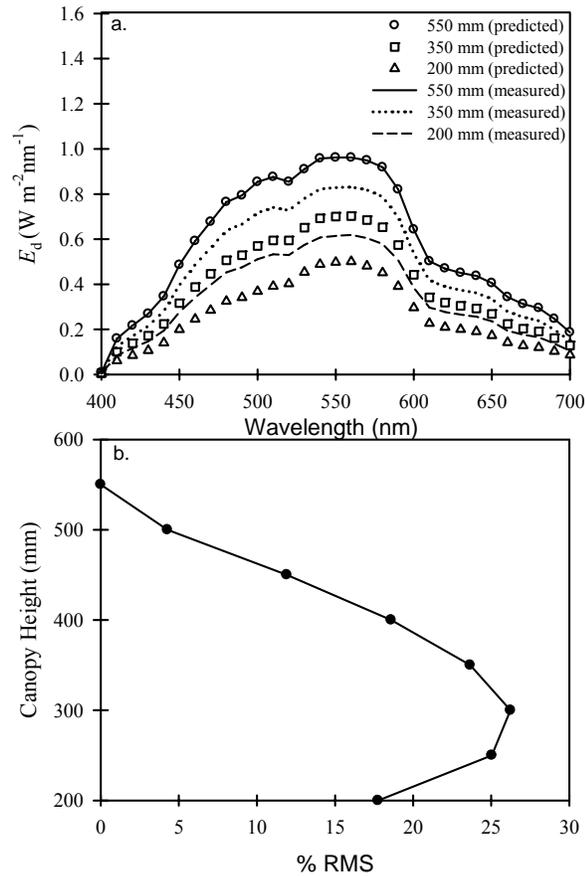
Figure 12. (a) Predicted vs measured downwelling irradiance (E_d) using the spherical

biomass distribution parameters after the canopy was assumed to take on a spherical

shape. **(b)** % RMS of predicted vs. measured (E_d) using the spherical canopy model.

Modeled upwelling irradiance (E_u) (Fig. 13a) was in best agreement with the measured upwelling irradiance at the top of the canopy. The % RMS error of 21% (Fig. 13b) was 13% less than the fully extended sigmoid model, and about 16% less than the compressed sigmoid models bent at 100, 300 and 500 mm, indicating that using the spherical model will best predict upwelling irradiance at the top of the canopy. The modeled upwelling irradiance in the middle of the canopy over predicted E_u relative to field measurements, with a % RMS error of 82%, which was 55% greater than the fully extended sigmoid model, and 24% less than the compressed sigmoid model bent at 100 mm, 4% greater than the compressed sigmoid model bent at 300 mm, and was 58% greater than the compressed sigmoid model bent at 500 mm. The modeled $E_u(\lambda, z)$ at the bottom of the canopy was 184% higher than the measured and had a % RMS value that was higher than the original sigmoid model by 134% and also higher for the compressed model bent at 100 mm, 300 mm and 500 mm with a difference of 86%, 88%, and 126% respectively.
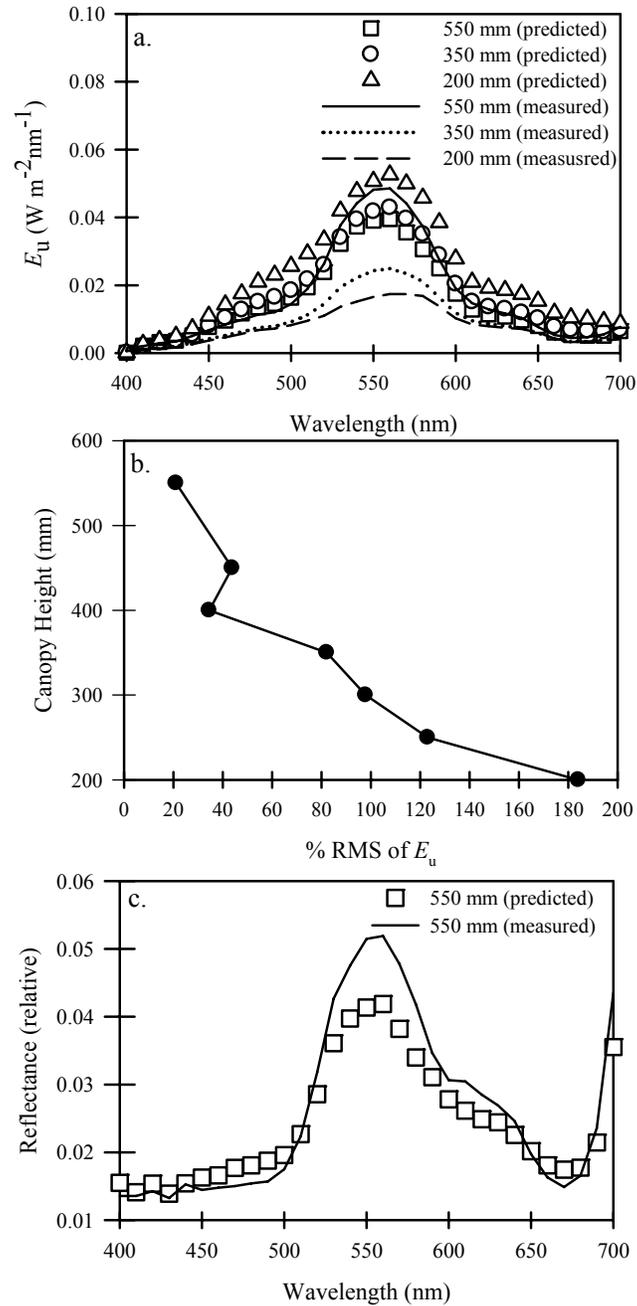
Figure 13 (a) Predicted vs measured downwelling irradiance (E_u) using the spherical

model biomass distribution parameters. **(b)** % RMS of predicted vs. measured E_u using

the spherical canopy model. **(c)** Predicted vs. measured reflectance (R) at the top of the

canopy.

Sensitivity of the spherical model to changes in $\overline{\mu}$ were also performed and compared to field measurements, but had a RMS error for both E_d and E_u of less than 0.5% at the top, middle and bottom of the canopy for a given biomass distribution, indicating that the model was not sensitive to changes in $\overline{\mu}$. Sensitivity of the model to $\overline{\mu}$ was chosen over other parameters because it is a main component, other than biomass distribution, that influences the way light is distributed within the canopy. This reinforces the importance of accurately parameterizing plant canopy architecture when evaluating radiative transfer in submerged plant canopies.

Predicting canopy reflectance as a function of L:

The accuracy of the spherical model to predict top of the canopy downwelling and upwelling light, allowed for the explanation of the relationship between whole canopy reflectance [$R_{TOC} = E_{u(TOC)}/E_{d(TOC)}$] at the top of the canopy and shoot density. Modeled reflectance for the top of the canopy was in good agreement with the measurements taken in the field with a % RMS error of 13% (Figure 13c). Agreement was even higher from 400 to 500 nm, as well as between 640 and 700 nm. Reflectance of the top of the seagrass canopy at peak reflectance (550 nm) (modeled and measured) was then plotted against *L* (Figure 14). There was no significant differences between the modeled and the measured regressions (ANCOVA, F = 0.04, P = 0.84, Table 2). As *L* increased, peak reflectance at 550 nm decreased because the fraction of bright sand reflectance contributing to R_{TOC} decreased.
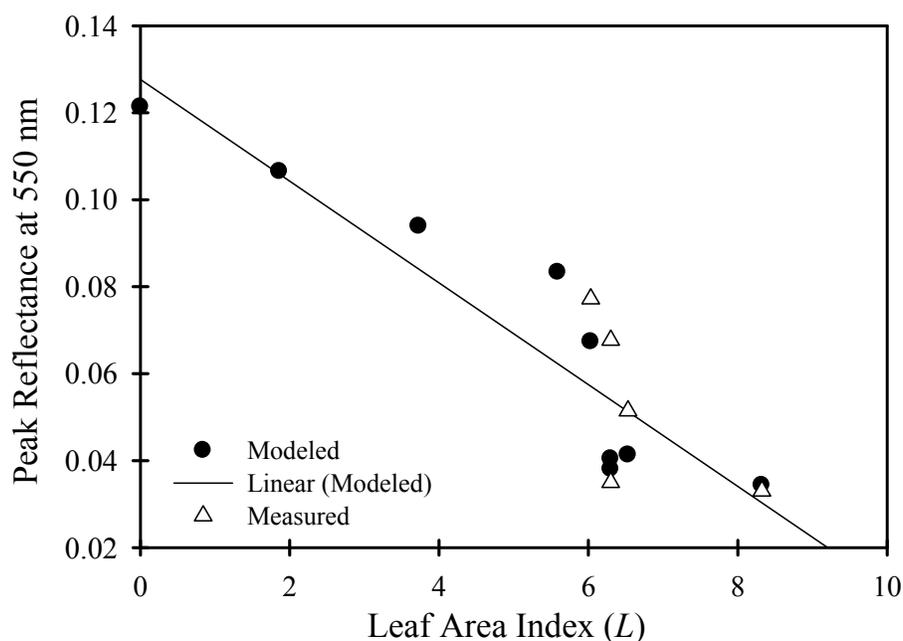
Figure 14. Leaf area index (L) vs peak reflectance at 550 nm (modeled and measured).

Table 2. ANCOVA of modeled vs. measured peak reflectances at 550 nm.

	SS	Degrees of Freedom	MS	F	p
Independent	0.000009	1	0.000009	0.0408	0.843684
Error	0.002508	11	0.000228		

Canopy photosynthesis, light-limited distribution, and depth distribution:

The light saturated rate of photosynthesis (P_m) for *S. filiforme* was 53 ± 17 μmol O_2 m^2 min^{-1} (Fig. 15). The initial slope (α) of the P vs. E curve was found to be 0.01 ± 0.006 (μmol O_2 evolved)/(μmol photon incident), the light saturation parameter (E_k) was found to be 82 ± 10 μmol photon m^{-2} sec^{-1}, the respiration rate was found to be 4 ± 2 μmol O_2 m^2 min^{-1}, and the P_g:R ratio was 15 ± 2.5 (Fig. 15). The oxygenic quantum

yield of photosynthesis (ϕ_p), the amount of O_2 evolved per photon absorbed, was also calculated by using the ratio of leaf photosynthesis to absorbed photosynthetically utilized radiation (*PUR*) was 0.14 ± 0.07 (μmol O_2 evolved)/(μmol quanta absorbed) which is not significantly different than the theoretical maximum value of 0.12 (= 1 mol O_2 evolved / 8 mol photons absorbed).

Figure 15. Gross Photosynthesis vs. Irradiance for *Syringodium filiforme*.

Effect of different model scenarios and shoot density on canopy productivity:

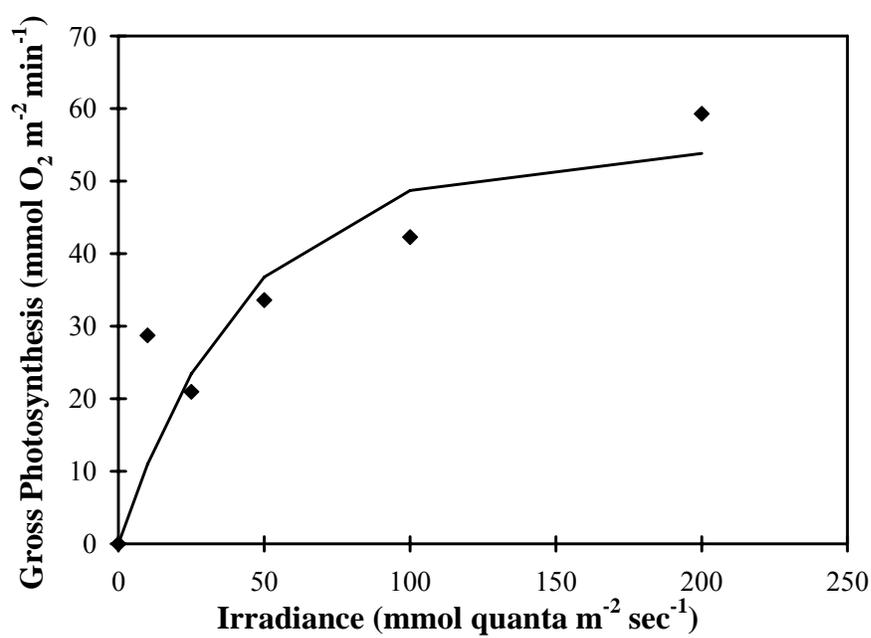Canopy productivity predicted by the spherical model was relatively the same as the extended sigmoid model's predictions. However, the compression model's predictions of canopy productivity were considerably lower than predictions of the spherical and the sigmoid model. Both the original sigmoid model and the spherical model predicted daily productivity for the canopy (P), of 10.2 ± 0.7. In contrast, the compressed sigmoid model bent at 100 and 300 mm had spectral daily productivity predictions of 4.3 ± 0.2. However, the compressed sigmoid model bent at 500 mm had similar spectral daily productivity predictions to that of the sigmoid and spherical model of $P = 10.4 \pm 0.4$. Therefore, the sigmoid model, the spherical model, and the compressed sigmoid model bent at 500 mm all predicted much higher rates of daily production than the compressed sigmoid model bent at 100 and 300 mm. Predictions of $P{:}R$ (spectral canopy $P{:}R$, per day), followed this same pattern with the sigmoid, compressed sigmoid model bent at 500 mm, and spherical model all predicting similar ratios of $P{:}R = 2.0 \pm 0.03$, and the compressed sigmoid model bent below 500 mm predicting much lower $P{:}R$ ratios of $P{:}R = 1.0 \pm 0.2$. Therefore, the compressed sigmoid model bent below 500 mm lowered productivity estimates by almost 50% for both daily productivity and canopy $P{:}R$.

As the canopy density was increased in the model simulation, the canopy production rates, or the spectral $P{:}R$ ratios decreased nonlinearly. The predicted light limited density, or when $P{:}R =1$, occurred at a shoot density of 5570 shoots m^{-2} with a maximum canopy height of 550 mm and a leaf area of 0.0047 m^2 shoot^{-1} during the model runs (Figure 16). However, measured shoot densities for *S. filiforme* ranged from 1600 to

2500 shoots m^{-2} and were well under the predicted light limitation of 5570 shoots m^{-2}, indicating that the meadows were not light limited (during the summer when the field measurements were made).
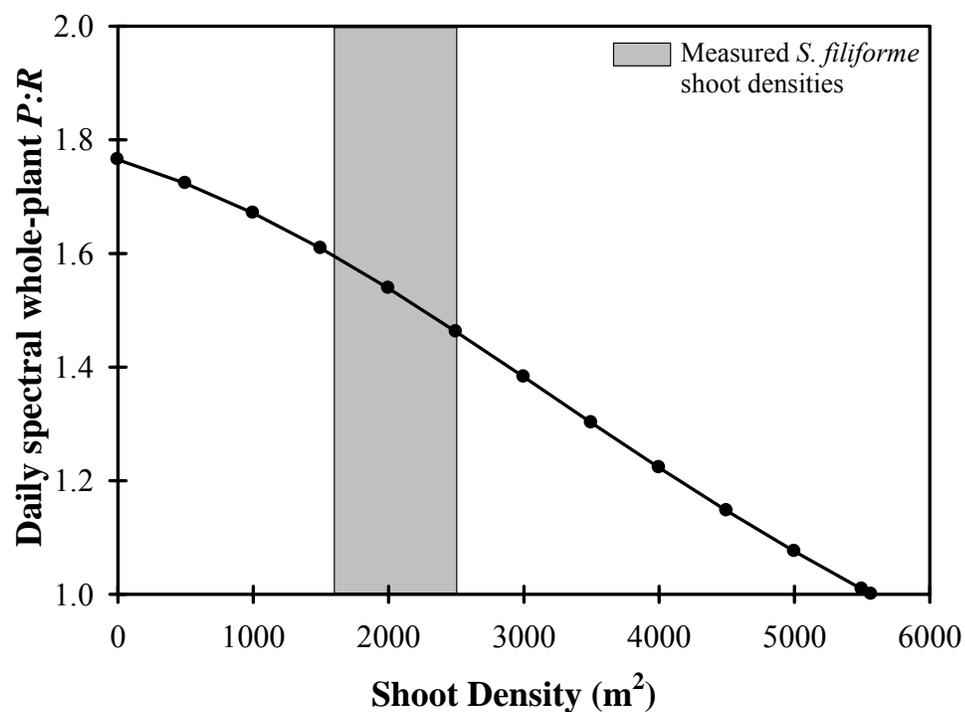
Figure 16. Shoot density vs daily spectral whole-plant *P:R*. Measured shoot densities for *Syringodium filiforme* ranged from 1600-2500 shoots m^{-2} (grey box). Predicted light limitation however, did not occur until the density reached 5570 shoots m^{-2}.

Effects of PUR-based estimates of shoot density and optical depth:

The maximum shoot density (where *P:R* = 1) for all *S. filiforme* stations based on *PUR* was strongly related to optical depth (r^2_{PUR} = 0.85). The optical depth of 2.4 is considered to be in the mid-point of the euphotic zone, and represents 10% of the incoming light [$E_d(0)$] from the surface, available for seagrasses and is commonly recognized as the threshold for seagrass survival (Figure 17), (Duarte, 1991). Model results suggested that the optical depth (ζ), where $\zeta = K_d z$, was less than 2.4 for *S. filiforme*, and therefore, support the commonly recognized threshold for seagrass survival.

Figure 17. Optical depth vs modeled maximum shoot density when *P:R* = 1 using *PUR*.

CHAPTER IV

DISCUSSION

The unique vertical biomass distribution of the *S. filiforme* canopy sets it apart from other seagrass species because much of the biomass originates in the middle of the canopy, rather than the bottom. This creates a unique biomass distribution that must be quantified to provide the best overall description of total light absorption and scattering by the submerged plant canopy. Although upwelling irradiances improved with the spherical model, downwelling irradiances predicted 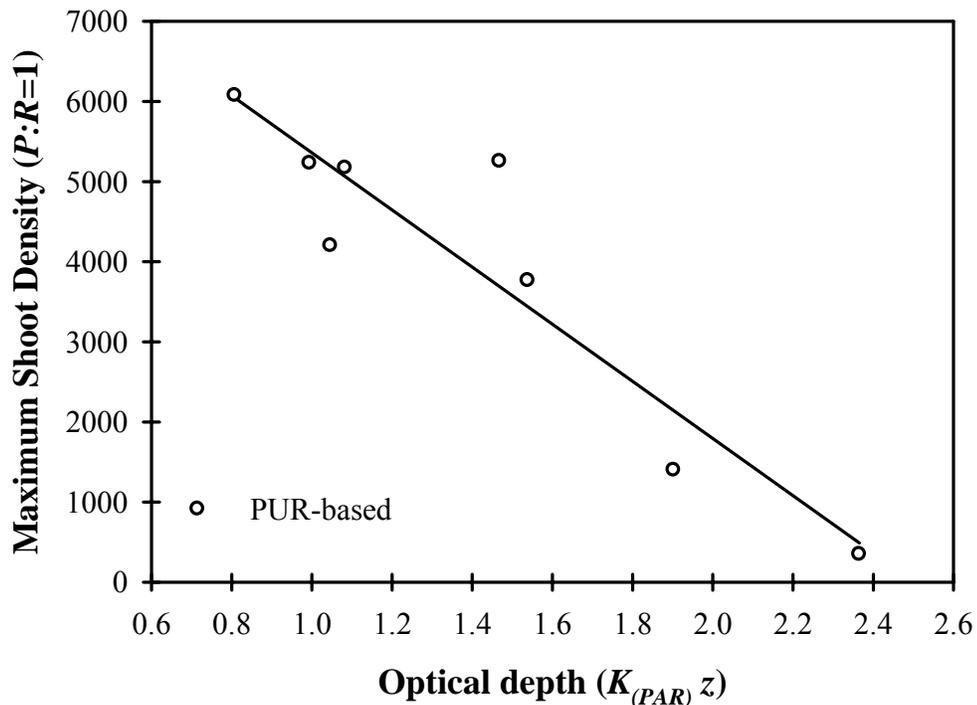only slightly higher % RMS values than the original sigmoid model, indicating that the sigmoid model and spherical models predict E_d with roughly equivalent accuracy. In fact, predictions of spectral daily production of the entire plant canopy and *P:R* were similar for the original sigmoid model, the sigmoid model compressed to 500 mm, as well as the spherical model, suggesting that use of any of these 3 models would give accurate estimates of productivity. However, the spherical model provides a more realistic representation of biomass distribution of the *S. filiforme* canopies characterized by its undifferentiated branching pattern. In contrast, predictions of spectral daily production and *P:R*, when using the compressed model bent at heights less than 500 mm, gave about 50% lower estimates, suggesting some sensitivity of the production estimates to canopy architecture.

The epifluorescent images of leaf cross-sections showed obvious differences in internal leaf anatomy between the round *S. filiforme* leaves and the flat leaves of *T. testudinum*. The chloroplasts of *S. filiforme* are distributed throughout the mesophyll and epidermis, while the chloroplasts of *T. testudinum* are tightly packed within a single

epidermal layer. Photosynthetic leaf absorptance $[A_L(\lambda)]$ spectra for *S. filiforme* differed from the $[A_L(\lambda)]$ for *T. testudinum* and *Z. marina* by about 40% (Cummings and Zimmerman, 2003). The more diffuse distribution of chloroplasts throughout the leaf, along with the higher amount of lacuanal space, significantly enhance internal scattering within the leaf, lowering the photosynthetic absorptance and increasing the non-photosynthetic absorptance. The high density of chloroplasts within the epidermis of *T. testudinum* maximizes their exposure to light, even at the expense of the package effect, allowing the photosynthetic absorption of *T. testudinum* and *Z. marina* to be high. Consequently, the diffuse distribution of chloroplasts within the mesophyll and epidermal cells of *S. filiforme* may reduce the package effect (increase chlorophyll light harvesting efficiency) relative to *T. testudinum* and *Z. marina*.

The lack of an obvious green "window" in the absorption spectra also may be a consequence of the unique structure of the *S. filiforme* leaf. Ramus (1978) observed similar differences in the absorption spectra between the thallus of *Ulva lactuca* and the thicker, cylindrical shaped thallus of *Codium fragile,* and suggested that these differences were due to the complex internal structures in *C. fragile* that promote light scattering and increase the probability of photon absorption. These findings may allow one to conclude that *S. filiforme* leaves maximize their light capture due to scattering of light within their complex internal features, particularly within their large, radialy arranged lacunae that create unavoidable refractive boundaries that promote light scattering. This may explain why more of the incident light is absorbed (due to non-photosynthetic tissue) when compared to leaves of *T. testudinum* and *Z. marina* that capture light predominately due to chlorophylls *a* and *b* (photosynthetic tissue). The package effect reduces the

effectiveness of light absorption by photosynthetic pigments due to the self-shading of the chromophores between layers of chloroplasts in the leaf (Falkowski and Raven, 2007; Cummings and Zimmerman, 2003). Increasing the absorption efficiency of *S. filiforme* leaves due to multiple scattering within the tissues may counterbalance the package effect (Enriquez, 2005). However, increased scattering within the leaf appears to reduce the overall efficiency of photosynthetic light harvesting, and the relatively high fraction of light absorbed by non-photosynthetic processes is not due to the package effect (which is a measure of chlorophyll efficiency), but more likely as a result of the complex internal structure of the *S. filiforme* leaf.

Unlike the absorption spectra, the reflectance spectra for *S. filiforme*, *T. testudinum*, and *Z. marina* were all very similar across the visible (400-700 nm), including the characteristic peak in the green (525-650 nm) that results from the presence of chlorophylls *a* and *b*. The dramatic rise in reflectance in the NIR portion of the spectrum is known as the "red edge" (enhanced near-infrared reflectance) and is due to the presence of photosynthetic pigments absorbing the visible, but not the NIR radiation. Also, reflectance is primarily a near-surface phenomenon, while absorption depends on transmission through the leaf, suggesting that the complex internal structures of *S. filiforme* should not influence reflectance.

Branching of *S. filiforme* leaves in the middle of the canopy, rather than at the bottom, results in a biomass distribution that may also boost the canopy's efficiency for photosynthetic light capture used by reducing self shading and producing more evenly illuminated leaves. This boost in light capture efficiency can be seen when the spherical model was applied and compared to the compressed sigmoid model providing a 50%

higher productivity estimate. The leaves' extreme horizontal angular distribution of the

compressed sigmoid model reduces light transmission to the lower levels of the canopy,

whereas the leaf distribution of the spherical model appears to increase the chance that

light would be intercepted evenly throughout all levels (Russell et al., 1989). Valladares

and Percy (2000) suggested that differences in canopy architecture for different species of

plants is a result of habitat and depend on whether light capture must be maximized or

whether excess light must be avoided to prevent photoinhibition. In the case of seagrass,

maximization of light capture is essential and therefore, they must adjust canopy

architecture for their environment.

Zimmerman (2003) suggested that increasing the bending angle in the upper half

of *T. testudinum* and *Z. marina* canopies would improve the ability of the model to

simulate observed irradiance distribution within the canopy, and the simulations

performed here demonstrated that the model seems to be quite sensitive to biomass

distribution changes between modeled and measured, especially in the taller canopies of

Z. marina, the results of this study indicated that compression of the sigmoid canopy

reduced the agreement between modeled and measured within *S. filiforme* canopies. The

sigmoid model modified by compression of the canopy did not accurately simulate the

distribution of *S. filiforme* leaves that originate at various locations throughout the middle

of the canopy. The spherical model was able to predict downwelling irradiance at the

middle and bottom of the canopy as well as upwelling irradiance at the top of the canopy,

which means that it also provides a reasonable simulation of the photosynthetically

relevant irradiance distributions necessary to calculate primary production of *S. filiforme*.

Self shading within the canopy may have caused the compression model's extreme

underprediction of downwelling irradiance and may have been the reason that the compressed sigmoid model resulted in much lower productivity estimates relative to the spherical model. Therefore, use of the spherical model can provide a robust tool for relating photosynthetic requirements of *S. filiforme* to water transparency, depth distribution and shoot density of natural populations in the field, as the sigmoid model has been shown effective for *T. testudinum* and *Z. marina* (Zimmerman, 2003, 2006).

Incident upwelling light in all layers of the canopy (top, middle and bottom) represented only about 3% of the total light [$E_u(z) + E_d(z)$] in a given layer. Therefore, underestimation of E_u by the model had trivial impact on canopy photosynthesis that has a measurement uncertainty of 32% ($P_m = 53 \pm 17$ μmol O_2 m^2 min^{-1}). Upwelling irradiances at all levels in the canopy were found to be below the reported value for E_k ($E_k = 82$ μmol photon m^{-2} sec^{-1}) with values of 24, 14, 11 μmol m^2 sec^{-1} at the top, middle and bottom of the canopy respectively at noon. However, values for downwelling irradiances were well above the reported E_k with values of 808, 678, 488 μmol m^2 sec^{-1} at the top, middle and bottom of the canopy, respectively at noon, indicating that at this time during the day in the summer, *S. filiforme* canopies were light saturated with respect to photosynthesis. Assuming a 12 hour day, along with applying the sun's angle in the sky as a sinusoidal function of time and day length, it was determined that E_d (TOC) begins to exceed the light saturation threshold (E_k) about 22 minutes after sunrise, and drops below E_k about 22 minutes before sunset. Thus, for 93% of the day, these *S. filiforme* canopies are light saturated and are light limited only 6% of the day and also suggest that E_u can be considered insignificant with respect to canopy photosynthesis.

The maximum rate of light-saturated photosynthesis exhibited by *S. filiforme* is similar to that of *Z. marina* (Dennison and Alberte, 1985; Zimmerman et al. 1995) and *T. testudinum* during the winter months (Herzka and Dunton, 1997) but only about 20% of the summertime rate. Also, because this population of *S. filiforme* was found to be operating near the theoretical limit for quantum yield (ϕ_p= 0.12) (Falkowski and Raven, 2007), the measurements used for this study could provide a reasonable upper limit boundary for leaf optical properties that can lead to broadly accurate predictions of maximum canopy photosynthesis in the absence of actual field measurements of specific populations of *S. filiforme*.

The results also indicate that these *S. filiforme* populations in Florida Bay were growing at densities (1600-2500 shoots m^{-2}) well below light limitation (5570 shoots m^{-2}). However, these plants may become light limited during periods of higher turbidity which may occur during other times of the year, such as winter and could be calculated with the model using lower light levels and decreasing the day length.

Confidence in top of the canopy reflectance is crucial for the development of global algorhythims for remote sensing of seagrass abundances. Predicted reflectances for the top of the canopy (defined as $R_u(\lambda,z) = E_u(\lambda,z) /E_d(\lambda,z)$) were in good agreement with modeled reflectance. This is crucial because there is a strong relationship between top of the canopy reflectance and *L* that could be exploited for remote sensing quantification of seagrass abundance. After correcting for the effects of the overlying water column, the optical signature of *S. filiforme* or any other benthic vegetation, top of the canopy reflectance can be retrieved and used for remote sensing purposes (Dierssen et al., 2003; Hill et al., in prep.). However, because reflectance spectra for *S. filiforme* are

similar to that of other seagrasses, it may be difficult to distinguish different species of

seagrasses from their optical signatures alone.   However, it is feasible to predict

quantitative measurements of seagrass L which, in turn, can be related to the amount of

productivity within a particular seagrass bed (Dierssen et al., 2003, Hill et al., in prep.).

CHAPTER V

CONCLUSION

The unique internal and external physical characteristics observed for *S. filiforme*, required significant modifications of the original bio-optical model developed by Zimmerman (2003) for *T. testudinum* and *Z. marina*. The model proved to be very sensitive to changes in biomass distribution and bending angles within the canopy, but not sensitive to other parameter changes such as $\bar{\mu}$, which controls the angle of distribution of the submarine light field. This model also suggests the use of a spherical biomass distribution within these canopies to provide a good estimate of downwelling (throughout the entire canopy) and upwelling irradiance at the top of the canopy. This model also provides estimates of spectral daily production as well as estimates of how increases in L would cause *S. filiforme* canopies to become light limited. These results would become useful for coastal managers to predict sudden declines in biomass due to sudden changes in environmental conditions. A good relationship between top of the canopy reflectance and L was determined with this model, and could become beneficial for the remote sensing community to provide coastal managers with quantitative measurements of seagrass abundance. Overall, understanding the biomass distribution within any vegetative canopy and incorporating this understanding into plant bio-optical models of light distribution and productivity, can provide essential tools for the remote sensing, coastal and environmental communities.

REFERENCES

Campbell, G., and J. Norman. 1998. An introduction to environmental Biophysics. Springer.

Campbell, J. B. 2006. Introduction to remote sensing. 4th ed. Guilford Press.

Cummings, M., and R. Zimmerman. 2003. Light harvesting and the package effect in the seagrasses *Thalassia testudinum* Banks ex Konig and *Zostera marina* L.: optical constraints on photoacclimation. Aquat. Bot. **75:** 261-274.

Daughtry, C., K. Ranson, and L.Biehl. 1989. A new technique to measure the spectral properties of conifer needles. Remote Sens. of Environ. **27:** 81-91.

Dennison, W., R. Orth, K. Moore, J. Stevenson, V. Carter, S. Kollar, P. Bergstrom, R. Batiuk. 1993. Assessing water quality with submerged aquatic vegetation: habitat requirement as barometers of Chesapeake Bay health. Bio-Science. **43:** 86-94.

Dennison, W., and R. Alberte. 1985. Role of daily light period in the depth distribution of *Zostera marina* (eelgrass). Mar. Ecol. Prog. **25:** 51-61.

Dierssen, H. M. and R.C. Zimmerman. 2003. Ocean color remote sensing of seagrass and bathymetry in the Bahamas Banks by high-resolution airborne imagery. Limnol. Oceanogr. **48:** 444-455.

Duarte, C. M. 1991. Seagrass depth limits. Aquat. Bot. **40, no.1:** 363-377.

Enriquez, S. 2005. Light absorption efficiency and the package effect in the leaves of the seagrass *Thalassia testudinum*. Marine Ecology Progress Series. **289:** 141-150.

Falkowski, P., and J. Raven, 2007. Aquatic Photosynthesis. 2nd Edition. Princeton
    University Press.

Hall, M., M. Durako, J. Fourqurean, and J. Zieman. 1999. Decadal Changes in Segrass
    Distribution and Abundance in Florida Bay. **22**: 444-459.

Hemminga, M.A., and C. Duarte. 2000. Seagrass Ecology. Cambridge Univ. Press.

Herzka, S., and K. Dunton. 1997. Seasonal photosynthetic patterns in the seagrass
    Thalassia testudinum in the western Gulf of Mexico. Mar. Ecol. Prog. Ser. **152**:
    103-117.

Hill, V., R. Zimmerman, P. Bissett, and H. Dierssen. In prep. Ocean color remote sensing
    of seagrass meadows in Saint Josephs Bay, Florida, by hyperspectral airborne
    imagery.

Hirose, T., and M. Werger. 1995. Canopy structure and photon flux partioning among
    species in an herbaceous plant community. Ecology. **76**: 466-474.

Kenworthy, J., and M. Fonesca. 1996. Light requirements of seagrasses *Halodule
    wrightii* and *Syringodum filiforme* derived from the relationship between
    diffuse light attenuation and maximum depth distribution. Estuaries. **19**: 740-
    750.

Kenworthy, J, and A. Schwarzschild. 1998. Vertical growth and short-shoot
    demography of *Syringodium filiforme* in outer Florida Bay, USA. Marine
    Ecology Progress Series. **173**: 25-37.

Kirk, J.T.O. 1994. Light & photosynthesis in aquatic ecosystems. 2nd Edition.
    Cambridege Univ. Press.

Lee, D. 1986. Unusual strategies of light absorption in rain-forest herbs. In T.J.

Givnish (editor), On the economy of plant form and function. Cambridge University Press. 105-131.

Longstaff, B., and W. Dennison. 1999. Seagrass survival during pulsed turbidity events: the effects of light deprivation on the seagrasses *Halodule pinifolia* and *Halophila ovalis*. Aquat. Bot. **65**: 105-121.

Louchard, E., R. Leathers, and T. Downes. 2003. Optical remote sensing of benthic habitats and bathymetry in coastal environments at Lee Stocking Island, Bahamas: A comparative spectral classification approach. **48**: 511-521.

Mobley, C.D. 1994. Light and Water : Radiative Transfer in Natural Waters. Academic Press.

Palacios, S., R. Zimmerman. 2007. Response of eelgrass *Zostera marina* to CO_2 enrichment: possible impacts of climate change and potential for remediation of coastal habitats. Mar. Ecol. Prog. Ser. **344**: 1-13.

Ramus, J. 1978. Seaweed anatomy and photosynthetic performance: the ecological significance of light guides, heterogeneous absorption and multiple scatter. J. Phycol. **14**: 352-362.

Russell, G., P. Jarvis, J. Monteith. 1989. Radiation absorption by canopies and stand growth. Plant canopies: their growth, form and function. Cambridge University Press. 21-39.

Short, F.T., S. Wyllie-Echeverria. 1996. Natural and human-induced disturbance of seagrasses. Environ. Conserv. **23**: 17-27.

Valladares, F., R. Pearcy. 2000. The role of crown architecture for light harvesting carbon gain in extreme light environments assessed with a realistic

3-D model. Anales Jard. Bot. Madrid. **58**: 3-16.

Verhoef,W., H. Bach. 2007. Coupled soil-leaf-canopy and atmosphere radiative

transfer modeling to simulate hyperspectral multi-angular surface reflectance

and TOA radiance data. Remote Sens. Environ. **109**: 166-182.

Vermaat, J.E., N. Agawin, C. Duarte, M. Fortes, N. Marba, J. Uri. 1995. Meadow

maintenance, growth and productivity of a mixed Philippine seagrass bed.

Mar. Ecol. Prog. Ser. **124**: 215-225.

Zimmerman, R.C. 2003 A biooptical model of irradiance distribution and

photosynthesis in seagrass canopies. Limnol. and Oceanogr. **48**: 568-585.

Zimmerman, R.C. 1995. Eelgrass (*Zostera marina* L.) transplants in San Francisco

Bay: Role of light availability on metabolism, growth and survival. Aquat.

Bot. **51**: 67-86.

Zimmerman, R.C. 1987. Evaluation of variance approximation techniques for non-

linear photosynthesis-irradiance models. Mar. Biol. **95**: 209-215.

Zimmerman, R., D. Kohrs, D. Steller, R. Alberte. 1997. Impacts of CO_2, enrichment

on productivity and light requirements of eelgrass. Plan. Physiol. **115**: 599-

607.

Zimmerman, R.C. 2006. Light and photosynthesis in seagrass meadows. *Seagrasses:*

Biology, Ecology and Conservation. Springer.

Zimmerman, R., A. Dekker. 2006. Aquatic Optics: Basic concepts for understanding

how light affects seagrasses and makes them measurable from space.

Seagrasses: Biology, Ecology and Conservation. Springer.